How did the foreland react? Yangtze foreland fold-and-thrust belt deformation related to exhumation of the Dabie Shan ultrahigh-pressure continental crust (eastern China)

Jens C. Schmid[1]* Lothar Ratschbacher[1], Bradley R. Hacker[2], Ines Gaitzsch[1] and Shuwen Dong[3]
[1]*Institut für Geologie, Technische Universität Bergakademie Freiberg, D-09596 Freiberg, Germany,* [2]*Department of Geological Sciences, University of California, Santa Barbara, CA 93106, USA,* [3]*Institute of Geomechanics, Chinese Academy of Geological Sciences, 100081 Beijing, P.R. China*

ABSTRACT

During the Triassic collision of the Yangtze and Sino-Korean cratons, the leading edge of the Yangtze crust subducted to mantle depths and was subsequently exhumed as a penetratively deformed, coherent slab capped by a normal shear zone. This geometry requires a reverse shear zone at the base of the slab, and we suggest that the Yangtze foreland fold-and-thrust belt constitutes this zone. Lower Triassic rocks of the eastern foreland record NW–SE compression as the oldest compressional stress field; onset of related deformation is indicated by Middle Triassic clastic sedimentation. Subsequent Jurassic stress fields show a clockwise change of compression directions. Based on nearly coeval onset and termination of deformation, and on a common clockwise change in the principal strain/stress directions, we propose that the foreland deformation was controlled by the extrusion of the ultra high-pressure slab. Widespread Cretaceous–Cenozoic reactivation occurred under regional extension to transtension, which characteristically shows a large-scale clockwise change of the principal extension directions during the Lower Cretaceous.

Terra Nova, 11, 266–272, 1999

Introduction

The Hong'an-Dabie-Sulu area in eastern China (Fig. 1) is the world's largest outcrop of continental crust affected by ultra high-pressure (UHP) metamorphism (e.g. Ames *et al*., 1996; Hacker *et al*., 1996; Liou *et al*., 1996). It forms the eastern part of the Qinling orogen and resulted from attempted Triassic subduction of the Yangtze craton beneath the Sino-Korean craton. Recent structural, petrological, and geochronological data (Rowley and Xue, 1996; Rowley *et al*., 1997; Hacker *et al*., in press) suggest an extrusion model for exhumation which has a reverse shear zone along the base and a normal shear zone along the top of the exhuming slab (see model of Chemenda *et al*., 1995). The normal shear zone was identified as comprising the crystalline core of Hong'an-Dabie capped by the Huwan detachment zone in Hong'an (Webb *et al*., 1999; Hacker *et al*., in press); it was reactivated in northern Dabie as the Xiaotian–Mozitang shear/fault zone in the Cretaceous (Fig. 1; Ratschbacher *et al*., in press).

*Correspondence: Institut für Geologie, Technische Universität Bergakademie Freiberg, D-09596 Freiberg, Germany, Tel.: + 49/3731393758, Fax: + 49/373139-3597; E-mail: jschmid@geo.tu-freiberg.de

The contractional deformation zone along the base of the exhuming slab has so far not been discussed in detail. Here we suggest that it is constituted by the Yangtze foreland fold-and-thrust-belt (YFTB). If so, the Triassic–Jurassic deformation of the YFTB provides a record of the exhumation kinematics of the slab, independent of the buoyancy-controlled deformation in the orogenic interior. Analysis of the Triassic–Jurassic history is complicated by the ubiquitous Cretaceous–Cenozoic postcollisional deformation, which dominates the structural architecture of both the crystalline core and the foreland of Dabie. Our goal to highlight the exhumation kinematics thus also addresses postcollisional reactivation.

The Qinling–Dabie orogen was apparently offset from the Sulu belt by the Tan-Lu fault zone (Fig. 1), which currently is a dextral transtensional fault (Zhang *et al*., 1995; Ratschbacher *et al*., in press). In nearly all models for the Qinling–Dabie–Sulu belt the Tan-Lu fault plays a key role. Yin and Nie (1993), for example, proposed that it was a sinistral transfer zone during Early Triassic indentation of a Yangtze promontory into the Sino-Korean craton. So far only evidence for Cretaceous–Cenozoic activity is abundant (Ratschbacher *et al*., in press). As the Cenozoic cover hampers observation of the Tan Lu, regional stress-field estimates in the YFTB to the east of the fault may clarify its history.

We subdivided the YFTB into a western, southern, and eastern segment, in which fold axes trend ESE, E, and NE, respectively (Fig. 1); here we focus on the eastern segment. This segment comprises folded and faulted Sinian to Lower Triassic passive margin sedimentary rocks, deposited on crystalline basement of the Yangtze craton. Carbonates were deposited from the Lower Carboniferous to the Lower Triassic, but from the Middle Triassic onward, terrigenous lacustrine and fluviatile sedimentary rocks occurred. Alkaline volcanic rocks were extruded in the Late Jurassic. During the Early Cretaceous mostly diorites to syenites intruded the YFTB, while coeval red bed sedimentation lasted until the Eocene–Oligocene (e.g. Zheng, 1985).

Structural analysis

Our results are based on the interpretation of 1:200,000 and 1:500,000 geological maps of the Anhui Province and on field observations, in particular of outcrop-scale structural geometries, and mesoscale fault-slip data. The latter were collected in outcrops of known Lower Triassic to Upper Cretaceous stratigraphic age. Slip sense was constrained by calcite, quartz, and kaolinite fibres, stylolites, and Riedel shears

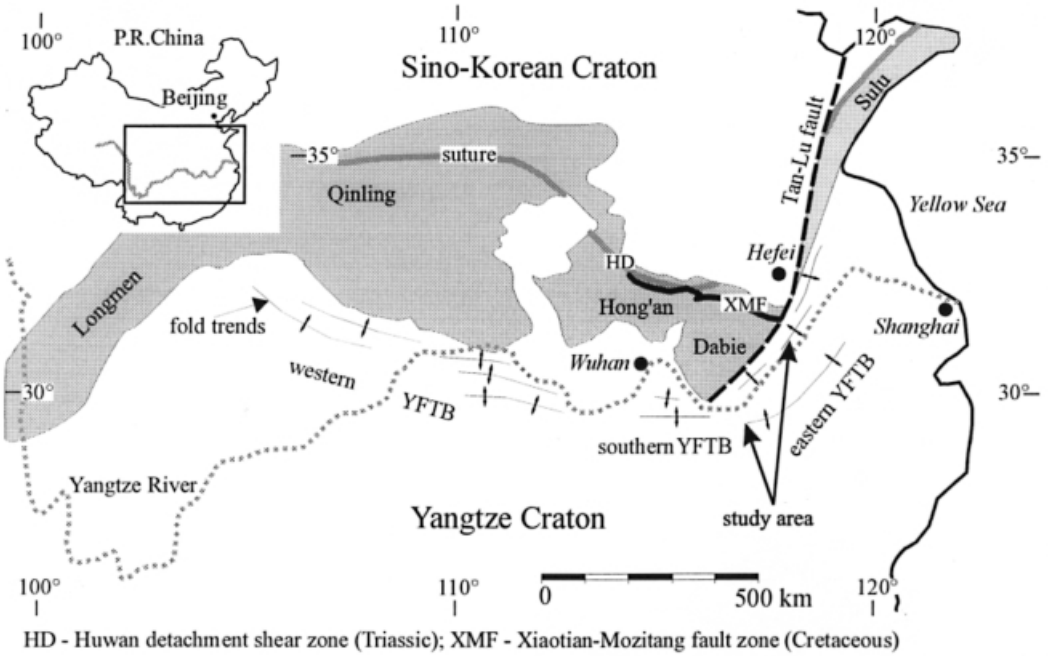

Fig. 1 Sketch map of the Qinling–Dabie–Sulu orogen (shaded), the Yangtze foreland fold-and-thrust belt (YFTB) and the main tectonic features. The Cretaceous Xiaotian–Mozitang fault zone is interpreted as the reactivated continuation of the Triassic Huwan detachment zone at the top of the exhuming ultrahigh-pressure slab.

on polished fault surfaces. The generally heterogeneous fault-striae datasets were divided into homogeneous subsets of different age based on cross-cutting relationships among faults and fibre growth and on the presence of curving fibres. The computer-program package of Sperner *et al*. (1993) was employed to calculate principal stress axes from the data of these subsets (Table 1, Table 2). These axes are interpreted to represent stress fields during different regional deformation events (e.g. Angelier, 1984). Due to the Cenozoic and Cretaceous overprint the pre-Cretaceous fields are less well constrained than the Cretaceous ones. In order to restore prefolding stress fields, rotations were carried out on some datasets; i.e. those sets that lack subvertical/subhorizontal stress axes after calculation were rotated to restore bedding to horizontal. If the rotation led to a subvertical (75–90°) stress axis, this subset was interpreted as a prefolding event.

Table 1 Location of stations and parameters of the deviatoric stress tensor: Triassic-Jurassic stress directions

Station	Lithology	Latitude (N)	Longitude (E)	#	σ_1	σ_2	σ_3	*R*	*F*
D572-Ta	limestone (T1)	30°45′20″	117°54′48″	03/03	327 52		167 36		
D572-Taro	limestone (T1)			03/03	148 19		291 67		
D572-Tb	limestone (T1)			01/01	337 10		101 80		
D573a1rot	limestone (T1)	30°49′31″	117°47′26″	01/01	318 02		056 75		
D573-a	limestone (T1)			05/05	144 02	054 02	278 87	0.5	17°
D573-b	limestone (T1)			07/07	187 16	009 74	278 00	0.6	18°
D576-a	limestone (T1)	31°30′18″	117°42′38″	03/03	310 02		217 52		
J15-ab	limestone (T1)	31°30′14″	117°51′52″	19/21	137 76	337 14	246 05	0.5	11°
J15-abrot	limestone (T1)			19/21	130 85	328 05	238 02	0.5	07°
J15-d	limestone (T1)			07/07	311 15	045 16	181 68	0.5	09°
J18-a	limestone (T1)	31°32′08″	117°44′42″	03/03	313 55		148 35		
J18-arot	limestone (T1)			03/03	320 05		138 85		
J18-b	limestone (T1)			08/08	332 10	067 28	224 60	0.5	10°
J20-a	limestone (T1)	31°26′45″	117°50′12″	03/03	177 03		267 03		
J5459-a	sandstone (J1)	30°49′46″	117°16′26″	17/17	014 04	199 86	104 00	0.6	18°

The numerical dynamic analysis method (Sperner *et al*., 1993) was used for calculation of principal stress directions ($\sigma_1 \leqslant \sigma_2 \leqslant \sigma_3$). For stations with fewer than four fault-slip data we report visually estimated contraction and extension directions. In the measurement column (#) first number is number of measurements used for calculation, second number gives total number of measurements. For σ_1–σ_3, azimuth (first number) and plunge (second number) of the principal stress axes are given. The stress ratio *R* is $(\sigma_2-\sigma_3)(\sigma_1-\sigma_3)^{-1}$ (where 1 is uniaxial confined extension, 0 is uniaxial confined compression). The fluctuation *F* gives the average angle between the measured slip and the orientation of the calculated theoretical shear stress.

Triassic–Jurassic deformation

Folds (Fig. 2, fold-axes diagram) and NW-striking faults that often show apparent sinistral and dextral displacements on the order of hundreds of metres are abundant at map-scale and occur in Palaeozoic to Lower Triassic rocks. Some of these faults are interpreted from sedimentary thickness variations as synsedimentary normal faults in T_1^3-limestone (T_1^3: upper Lower Triassic), indicating that normal faulting started before folding (see below). The inferred prefolding NE–SW extension is corroborated by en-echelon tension gashes and conjugate shear zones (Fig. 2, J15-tg, J18).

Table 2 Location of stations and parameters of the deviatoric stress tensor: Cretaceous stress directions

Station	Lithology	Latitude (N)	Longitude (E)	#	σ_1	σ_2	σ_3	*R*	*F*
D200old	orthogneiss (K1)	31°47′41″	117°33′16″	20/21	092 13	315 72	184 12	0.5	17°
D200you	red beds (K1)			13/13	093 71	268 19	358 02	0.4	17°
D201you	orthogneiss (K1)	31°28′24″	117°22′41″	10/10	118 19	346 63	215 19	0.4	24°
D201ys	volcanics (K1)			12/13	149 12	347 77	240 04	0.6	21°
D285you	limestone (P)	30°15′40″	116°23′20″	26/27	249 04	348 69	157 20	0.3	19°
D566-a	volcanics (J3)	30°27′37″ ξρ″	116°44′05″	11/11	020 63	180 25	274 08	0.6	17°
D566-b	volcanics (J3)			13/13	065 15	226 74	333 05	0.7	22°
D566-c	volcanics (J3)			15/15	036 87	134 00	224 03	0.8	22°
D570-ab	cherty marble	30°37′21″	117°05′01″	13/15	250 39	053 50	153 08	0.5	22°
D570-c	cherty marble			07/07	277 18	124 70	010 09	0.7	23°
D572Td	limestone (T1)	30°45′20″	117°54′48″	07/07	295 77	011 13	201 01	0.5	19°
D572KTa	fanglomerate (K2)			18/18	013 06	280 28	114 61	0.5	15°
D573-b	limestone (T1)	30°49′31″	117°47′26″	03/03	104 65		322 20		
D573-c	limestone (T1)			07/07	311 21	135 69	042 01	0.6	27°
D576-c	limestone (T1)	31°30′18″	117°42′38″	12/12	355 74	229 09	137 13	0.9	27°
D576-d	limestone (T1)			18/18	262 04	025 83	172 06	0.6	19°
J37-a	fanglomerate (J3)	30°55′29′	117°28′30″	04/04	248 20	091 68	341 08	0.5	09°
J5459-b	sandstone (J1)	30°49′46″	117°16′26″	09/09	235 13	042 76	144 03	0.5	19°
J5459-c	sandstone (J1)			04/04	007 68	237 14	143 16	0.5	11°
J5459-d	sandstone (J1)			09/09	277 15	041 65	181 20	0.4	18°
J5459-e	sandstone (J1)			14/14	325 03	078 82	234 08	0.5	12°
J62-a	marble	30°39′10″	117°05′23″	03/03	099 80		285 10		
J62-b	marble			06/06	220 09	351 76	128 10	0.9	11°
J69-c	limestone (P-T1)	30°35′25″	117°00′32″	07/07	081 70	182 04	274 20	0.5	13°
J76b	cherty marble	30°37′33″	116°51′50″	04/04	309 48	098 38	201 15	0.5	08°
J76brot	cherty marble			04/04	302 83	106 07	196 02	0.5	09°
J7879-a	sandstone (J1-J2)	30°24′20″	116°36′28″	04/04	004 69	170 21	262 05	0.5	19°
J7879-b	sandstone (J1-J2)			19/19	062 17	270 71	155 09	0.4	20°
J7879-c	sandstone (J1-J2)			08/08	321 06	122 83	231 02	0.7	20°

See Table 1 for explanation.

Several stations record layer-parallel shortening by faulting and folding predating the main, regional folding event (Fig. 2, e.g. D572, D573-a, J45, J18-a). This prefolding thrusting probably led to the emplacement of the thrust sheets in the Chaohu area, which are preserved in synclinal depressions as klippen of Sinian stromatolitic dolomite on top of T_1^3-limestone. The small-scale box folds at station J45 are not higher-order folds of a regional fold; their axial planes are subhorizontal within regional folds with subvertical axial planes. Rotation to horizontal bedding suggests a prefolding origin (Fig. 2).

Outcrop-scale grabens, striking perpendicular to the regional fold axes, show curving calcite fibres on their faults reflecting rotation of beds during faulting. We interpret these grabens to document fold-axis parallel extension (Fig. 2, e.g. J15-ab). Middle Triassic sedimentary breccia and conglomerate, composed of material from the sedimentary cover of the Yangtze craton and deposited unconformably on T_1^3-limestone, date the main folding phase. A comparison of prefolding with postfolding compression directions indicates a clockwise change from WNW to NW. Postfolding NW–SE compression, with an average σ_1 of 324 $\pm$ 13° in T_1^3-limestone ($\sigma_1 \geqslant \sigma_2 \geqslant \sigma_3$, principal stress directions; 6 stations), is documented both in T_1^3-limestone and J_1-sandstone (J_1, Lower Jurassic); in the latter the bedding-parallel slip (postfolding but pretilting, see later) direction was 331° (Fig. 2, J5459). These Jurassic sand-and siltstones, with abundant detrital white mica, most likely have their source in metamorphic basement rocks of the exhuming orogen. Subsequently, the compression direction rotated clockwise (from NW–SE to NNE–SSW) which is recorded in both Triassic (J20a, D573-b) and Jurassic (J5459-b) rocks. The NNE–SSW compression caused widespread N to NE tilting of Jurassic rocks and overprinting small-scale folds. This postfolding (related to the main folding phase) rotation of σ_1 is, for example, well recorded in the curving fibres at J18-b (Fig. 2).

Outcrop-scale folds (dm to m) show a wide range of fold-axis orientation (e.g. J20a, D573a1rot). We relate these deviations from the main NE-trend to the late-stage rotation of the compression direction. Whereas the onset of the compression is relatively well constrained to the Middle Triassic, its termination is less well known. We assume that it waned at the end of the Middle Jurassic, when clastic sedimentation ceased and volcanic rocks started to be extruded in the Upper Jurassic.

Cretaceous deformation

The intrusion of diorites to syenites into the sedimentary cover N and E of Anqing (Fig. 3) caused contact metamorphism and facilitated syn- to postintrusive ductile extensional deformation in cherty marble. Strong subhorizontal extension is reflected by a subhorizontal foliation and the formation of folds with fold-axis parallel stretching lineation (Fig. 3, J76a). The folds in these highly ductile rocks are interpreted to result from folding of initially steeply dipping Triassic rocks by subvertical shortening and subhorizontal stretching (model of Froitzheim, 1992). Similar structures were reported from localities several hundred km further to the south (Faure *et al.*, 1996, 1998). $^{40}Ar/^{39}Ar$ mica cooling ages of two granitoids in the southern YFTB (Ratschbacher *et al.*, in press) suggest that WNW–ESE extension started around 140 Ma. This stress field is also represented by NNE-striking mafic to intermediate dykes (e.g. J62-a, Fig. 3).

Subsequent deformation occurred mainly on E–W striking, sinistral transtensive faults. This fault set is subparallel to the 140–120 Myr-old (Ratschbacher *et al.*, in press) Xiaotian–Mozitang shear/fault zone of northern Dabie. Curving fibres on a large number of these faults indicate a continuous, clockwise change in the extension direction (NW–SE to NE–SW; Fig. 3). Fault-slip data in early Late Cretaceous (K_2) alluvial fan sediments (D572KTa) postdate the E–W- and NW–SE-orientated extensions and record NNE–SSW compression. NE–SW sinistral transpression along WNW-trending map-scale faults was post-Eocene and was probably related to the India–Asia collision (Peltzer *et al.*, 1985; Zhang *et*

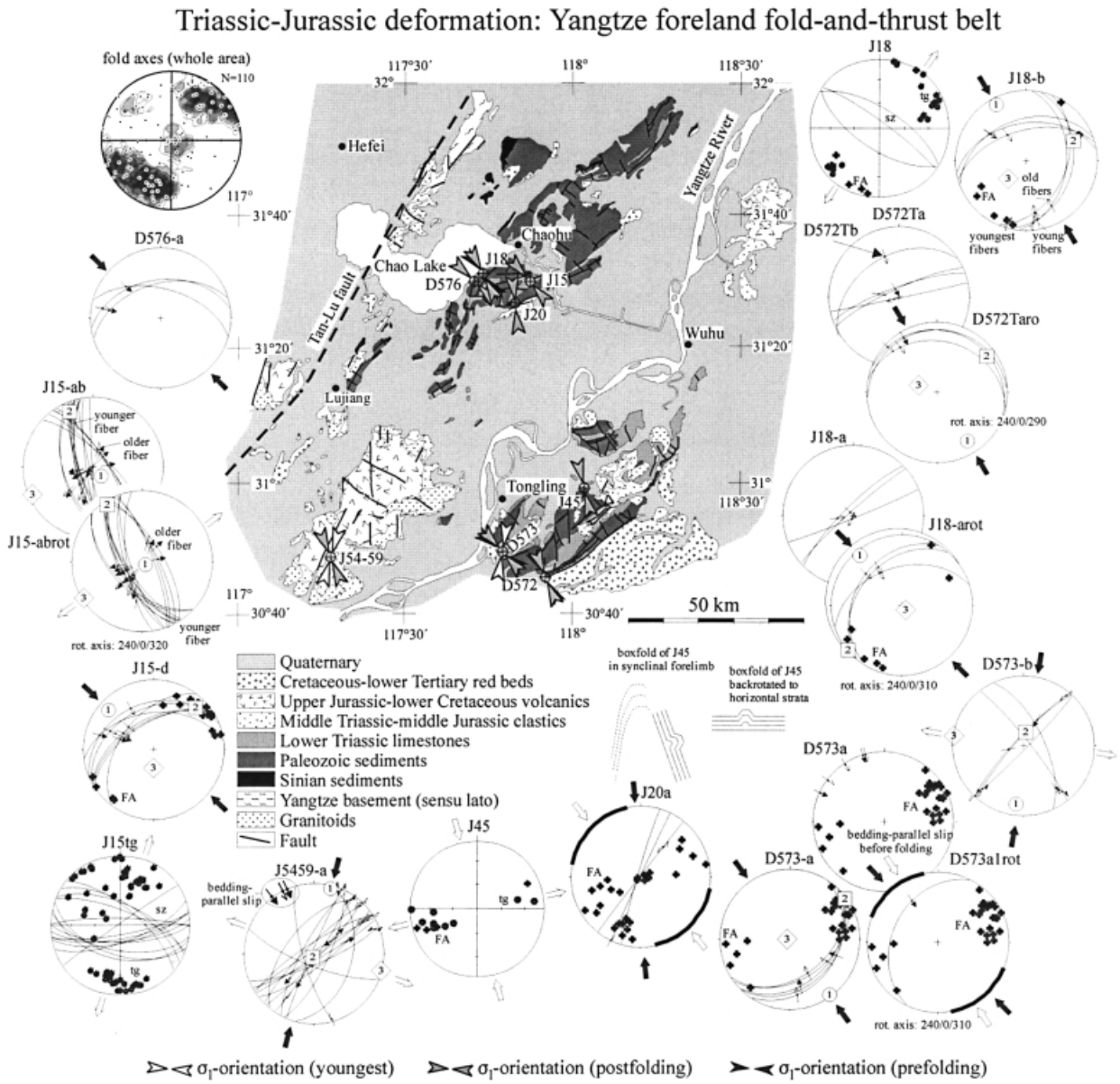

Fig. 2 Triassic–Jurassic deformation of the Yangtze foreland fold-and-thrust belt east of the Dabie Shan. Structural data are plotted in lower-hemisphere, equal-area projections. FA, fold axis; sz, shear zone; tg, tension gash. Great circles represent faults and solid, open, half, and headless arrows represent striae of certain, reliable, inferred, and unknown slip sense. This confidence scale was introduced to allow an assessment of the quality of the database. The clockwise change in the principal compression direction is recorded, for example, in stations J18, D573, D572, and J5459. Older, younger, and youngest 'fibres' highlight relative age of striae on the same fault. Overprinting, small-scale folds in the whole area fold-axes plot show NW–SE orientation. The full arrows outside the stereograms relate to principal stress directions ($\sigma_1 \geqslant \sigma_2 \geqslant \sigma_3$) calculated from fault-slip data, white arrows to contraction directions derived from fold orientations. Thick black lines at some stereograms highlight shortening-direction variability derived from the fold-axis orientation scatter. Rotated data are indicated with 'rot' in the station numbers and rotation axes (trend, plunge) and angles (°) are given below the stereograms.

al., 1995). Thus the NNE–SSW compression probably was Upper Cretaceous/Palaeocene; in this stress field, the Tan-Lu fault could have been active as a sinistral strike-slip fault.

We studied the Cretaceous near-field deformation of the Tan-Lu fault at two localities (Fig. 3). Quartz-ribbon mylonite (D200) formed below the quartz recrystallization temperature (~300 °C) along NE-striking dextral strike-slip imbricates within cataclastic granite (unpublished Chinese K/Ar whole rock age of 130 Myr) and Cretaceous red bed conglomerate; deformation continued into brittle faulting. Orthogneiss (D201) deformed during low-temperature cooling from 119 to 116 Ma ($^{40}Ar/^{39}Ar$ K-feldspar; Ratschbacher *et al*., in press), probably traces a younger (?sinistral) event.

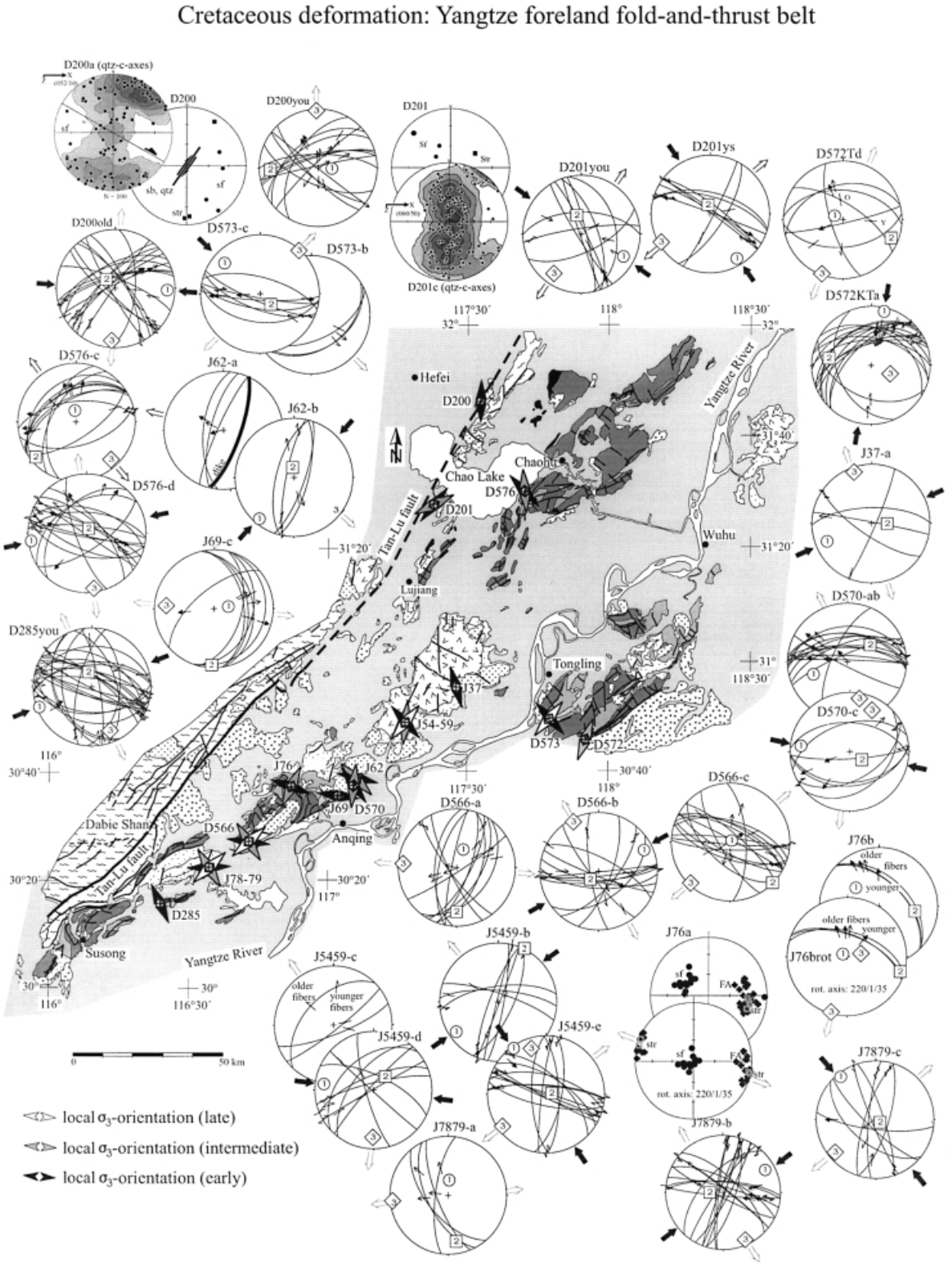

Fig. 3 Structural data (lower-hemisphere, equal-area projection) of Lower Cretaceous faulting (note the widespread change in stress direction orientations — from ESE–WNW to NE–SW), and the probably Upper Cretaceous–Palaeocene NNE–SSW compression. Several stations record Tan-Lu parallel sinistral transpressive faults (e.g. J5459-e, D572Kta). Contoured diagrams D200a and D201c show U-stage derived quartz *c*-axis textures (crystallographic preferred orientation), which are used to derive flow direction and in D200a additionally flow sense. For symbols, fault-slip data explanation, and legend see Fig. 2.

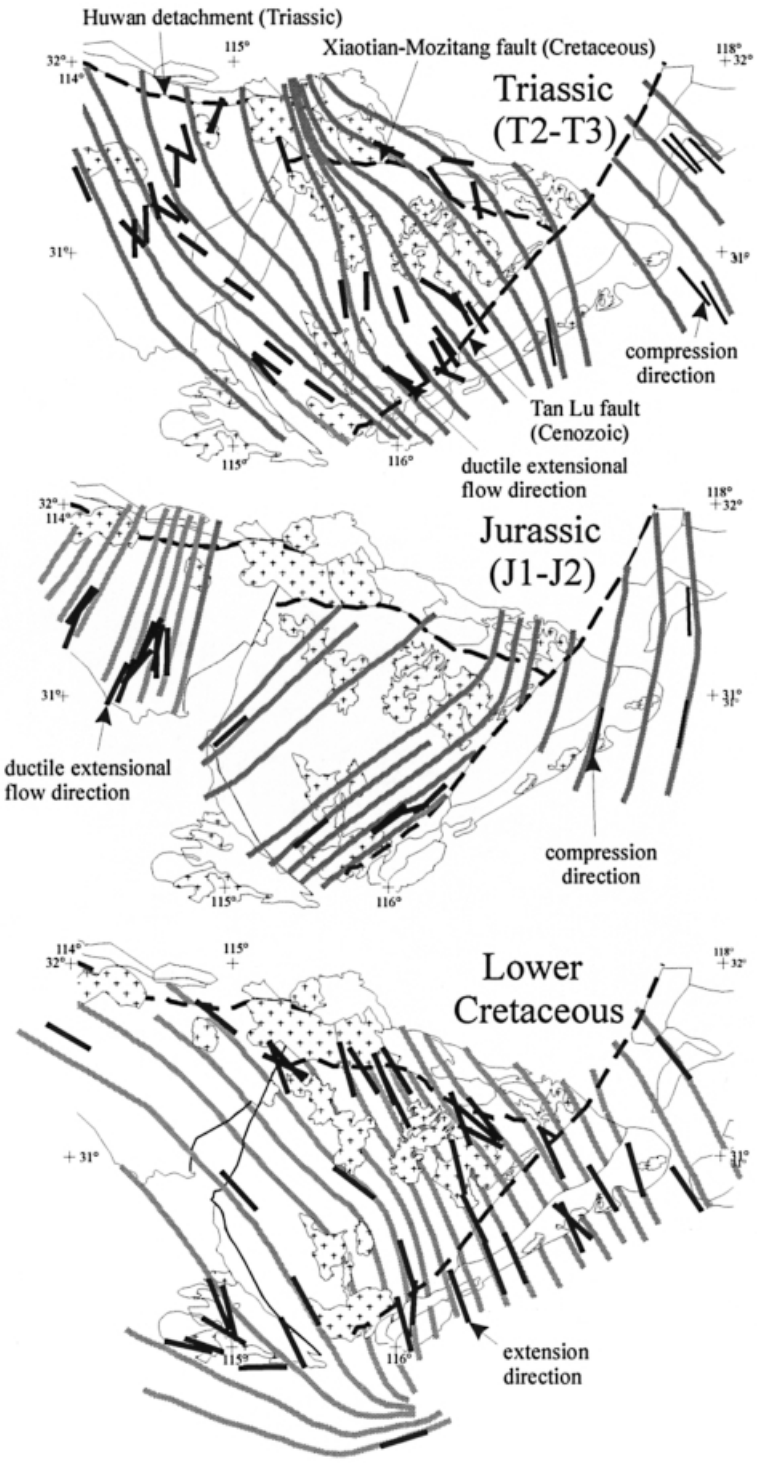

Fig. 4 Trajectory maps correlating, speculatively, coeval flow in the orogenic interior and faulting in the eastern Yangtze foreland fold-and-thrust belt (YFTB) for three different time periods. During the Triassic ductile flow in the orogen was top NW that was coeval with NW–SE compression in the eastern YFTB and dextral transpression in the southern and western YFTB (unpubl. results). The clockwise change of the principal strain/stress directions in the Jurassic affected both the crystalline core and the eastern YFTB. Lower Cretaceous NW–SE extension took place mainly along the sinistral Xiaotian–Mozitang fault zone; the dextral Tan-Lu is interpreted as a conjugated fault zone. The distance-weighting method of Lee and Angelier, (1994) was employed to produce regional trajectories from multiple local stress/strain orientation determinations.

Discussion and conclusions

The oldest contractional deformation in the Lower Triassic rocks of the YFTB east of Dabie occurred within a NW-trending (σ_1) compressional stress field, with layer-parallel shortening, thrusting, folding, and fold-axis parallel extension. Middle Triassic sedimentary breccia and conglomerate indicate the onset of folding. This stress field was in place throughout the deposition of Early Jurassic synorogenic siliciclastic rocks. Subsequent stress fields changed clockwise as recorded in both Triassic and Jurassic rocks; the final σ_1 orientation was NNE–SSW. Contractional deformation probably waned during the Middle Jurassic. It was certainly over in the Early Cretaceous, when extensional deformation was established.

Is foreland deformation related to exhumation in the orogenic interior? Figure 4 depicts trajectories of possibly coeval (within the age constraints established thus far) Triassic and Jurassic deformation in the orogen and its foreland. Our comparison of compressive stress orientations derived from low-strain brittle-faulting in the footwall of the exhuming slab, with high-strain ductile flow orientations within the slab in the orogenic interior, although highly speculative, may indicate that normal flow within the slab and contraction in the foreland were coeval and similarly orientated. The structural and geochronological work of Hacker *et al.* (1998; in press) implies that the slab exhumed towards the SE from mantle to crustal depths between 235 and 220 Ma; it rotated clockwise about a western pivot with a final S-directed component reflected by isotopic ages as young as 170 Myr. Although the details of the kinematics and timing within both the exhuming slab and the YFTB remain to be established, our preferred model proposes that the stress distribution in the YFTB was controlled by the extrusion of the UHP slab within Hong'an-Dabie. In this model the oroclinal fold bend of the YFTB resulted from the progressive exhumation kinematics of the orogen.

An alternative model relates the foreland deformation to the large relative clockwise rotation (up to 70°) of the colliding cratons during the Triassic–Jurassic (see palaeomagnetic data of Zhao and Coe, 1987; Enkin *et al.*,

1992; Gilder and Courtillot, 1997). These data are interpreted to reflect a 'scissor-like' closure of an oceanic basin between the Yangtze and the Sino-Korean cratons. This model, however, contradicts the reported Middle Triassic compressional deformation in the southern (Faure *et al*., 1998; own field studies) and western YFTB (Huang and Wu, 1992) where, at this time, oceanic subduction should have been active and compressional deformation younger, i.e. Middle Jurassic.

If the Tan-Lu fault existed during the Triassic–Jurassic, it probably would have been a thrust fault, and, at the end of exhumation history in the Middle Jurassic–in a NNE–SSW transpressive stress field–a sinistral strike-slip fault zone. Late Mesozoic reactivation throughout the Qinling–Dabie orogen and its foreland occurred within regional extensional to transtensional stress fields (Fig. 4), which characteristically show large-scale clockwise rotation of the principal extension directions during the Lower Cretaceous (Ratschbacher *et al*., in press; this study); transtension and extension probably took place in the whole Yangtze block (Faure *et al*., 1996), perhaps as a result of far-field collisions and Pacific subduction (Ratschbacher *et al*., in press). Deformation at two localities within the near field indicates that the Tan-Lu fault was probably conjugated to the sinistral transtensive Xiaotian–Mozitang shear/fault zone of northern Dabie, and thus was active between 140 and 120 Ma. In the uppermost Cretaceous/Palaeogene, during NNE–SSW transpression, the Tan-Lu fault might have been a sinistral strike-slip fault.

Acknowledgements

This study was funded by DFG grants Ra442/9, 14 and NSF grant EAR-9417958. Thanks to Robert Schmid and Laura Webb for discussions both in the field and the laboratory and to Johannes Pic and Hagen Deckert for transferring maps into computer graphics. Field discussions and logistical field support came from numerous Chinese colleagues; they made this research possible. The journal reviewers Michel Faure and An Yin are thanked for their stimulating comments.

References

Ames, L., Zhou, G. and Xiong, B., 1996. Geochronology and isotopic character of ultrahigh-pressure metamorphism with implications for collision of the Sino-Korean and Yangtze cratons, central China. *Tectonics*, **15**, 472–489.

Angelier, J., 1984. Tectonic analysis of fault slip data sets. *J. Geophys. Res*., **89**, 5835–5848.

Chemenda, A.I., Mattauer, M., Malavieille, J. and Bokun, A.N., 1995. A mechanism for syn-collisional rock exhumation and associated normal faulting: Results from physical modelling. *Earth Planet. Sci. Lett*., **132**, 225–232.

Enkin, R.J., Yang, Z., Chen, Y. and Courtillot, V., 1992. Paleomagnetic constraints on the geodynamic history of the major blocks of China from the Permian to the present. *J. Geophys. Res*., **97**, 953–989.

Faure, M., Sun, Y., Shu, L., Monié, P. and Charvet, J., 1996. Extensional tectonics within a subduction-type orogen. The case study of the Wugongshan dome Jiangxi Province, southeastern China. *Tectonophysics*, **263**, 77–106.

Faure, M., Lin, W. and Sun, Y., 1998. Doming in the southern foreland of the Dabieshan (Yangtze block, China). *Terra Nova*, **10**, 307–311.

Froitzheim, N., 1992. Formation of recumbent folds during synorogenic crustal extension Austroalpine nappes, Switzerland). *Geology*, **20**, 923–926.

Gilder, S. and Courtillot, V., 1997. Timing of the North–south China collision from new middle to late Mesozoic paleomagnetic data from the North China Block. *J. Geophys. Res*., **102**, 17,713–17,727.

Hacker, B.R., Wang, X., Eide, E.A. and Ratschbacher, L., 1996. Qinling–Dabie ultrahigh-pressure collisional orogen. In: *The Tectonic Evolution of Asia* (A. Yin and T.M. Harrison, eds), pp. 345–370. Cambridge University Press, Cambridge.

Hacker, B.R., Ratschbacher, L., Webb, L., Ireland, T., Walker, T. and Dong, S., 1998. U/Pb zircon ages constrain the architecture of the ultrahigh-pressure Qinling-Dabie orogen, China. *Earth Planet. Sci. Lett*., **160**, 215–230.

Hacker, B.R., Ratschbacher, L., Webb, L. *et al*., in press. Exhumation of ultrahigh-pressure rocks in east-central China: Late Triassic-Early Jurassic extension. *J. Geophys. Res*., in press.

Huang, W. and Wu, Z.W., 1992. The Evolution of the Qinling Orogenic Belt. *Tectonics*, **11**/**2**, 371–380.

Lee, J.C. and Angelier, J., 1994. Paleostress trajectory maps based on the results of local determinations: the 'LISSAGE' program. *Computers & Geosci*., **20**, 161–191.

Liou, J.G., Zhang, R.Y., Eide, E.A., Maruyama, S., Wang, X. and Ernst, W.G., 1996. Metamorphism and tectonics of high-P and ultrahigh-P belts in Dabie-Sulu Regions, eastern central China. In: *The Tectonic Evolution of Asia* (A. Yin and T.M. Harrison, eds), pp. 300–343. Cambridge University Press, Cambridge.

Peltzer, G., Tapponnier, P., Zhang, Z. and Xu, Z.Q., 1985. Neogene and Quaternary faulting in and along the Qinling Shan. *Nature*, **317**, 500–505.

Ratschbacher, L., Hacker, B.R., Webb, L. *et al*., in press. Exhumation of the ultrahigh-pressure continental crust in east-central China: Cretaceous and Cenozoic unroofing and the Tan-Lu fault. *J. Geophys. Res*., in press.

Rowley, D.B. and Xue, F., 1996. Modeling the exhumation of ultra-high pressure metamorphic assemblages; observations from the Dabie/Tongbai region, China. *Geol. Soc. Am. Abstr*., **28**, 249.

Rowley, D.B., Xue, F., Tucker, R.D., Peng, Z.X., Baker, J. and Davis, A., 1997. Ages of ultrahigh pressure metamorphism and protolith orthogneisses from the eastern Dabie Shan: U/Pb zircon geochronology. *Earth Planet. Sci. Lett*., **151**, 191–203.

Sperner, B., Ratschbacher, L. and Ott, R., 1993. Fault-striae analysis: a Turbo Pascal program package for graphical representation and reduced stress-tensor calculation. *Computers & Geosci*., **19**, 1361–1388.

Webb, L.E., Hacker, B.R., Ratschbacher, L., McWilliams, M.O. and Dong, S., 1999. $^{40}Ar/^{39}Ar$ thermochronologic constraints on deformation and cooling history of high and ultrahigh-pressure rocks in the Qinling-Dabie orogen. *Tectonics*, **18/4**, 621–638.

Yin, A. and Nie, S., 1993. An indentation model for the North and South China collision and the development of the Tan-Lu and Honam fault systems, eastern Asia. *Tectonics*, **12**, 801–813.

Zheng, X., 1985. Meso-Cenozoic volcanic rocks in east China and adjacent areas with relation to plate tectonics. *Tectonophysics*, **112**, 533–550.

Zhang, Y.Q., Vergely, P. and Mercier, J., 1995. Active faulting in and along the Qinling Range (China) inferred from SPOT imagery analysis and extrusion tectonics of south China. *Tectonophysics*, **243**, 69–95.

Zhao, X.X. and Coe, R.S., 1987. Paleomagnetic constraints on the collision and rotation of north and south China. *Nature*, **327**, 141–144.

Received 7 May 1999; revised version accepted 10 January 2000

